Electronic Supplementary Material (ESI) for Polymer Chemistry.

Supporting Information

Polycondensation in Confined Nanopores toward Selective Formation of Narrowly Dispersed Linear Polyesters

Xiaowang Yu, Baojun Li, Jie Wang, Zhikun Shang, Donglai Tian, Guiyou Wang* and Aiguo Hu*

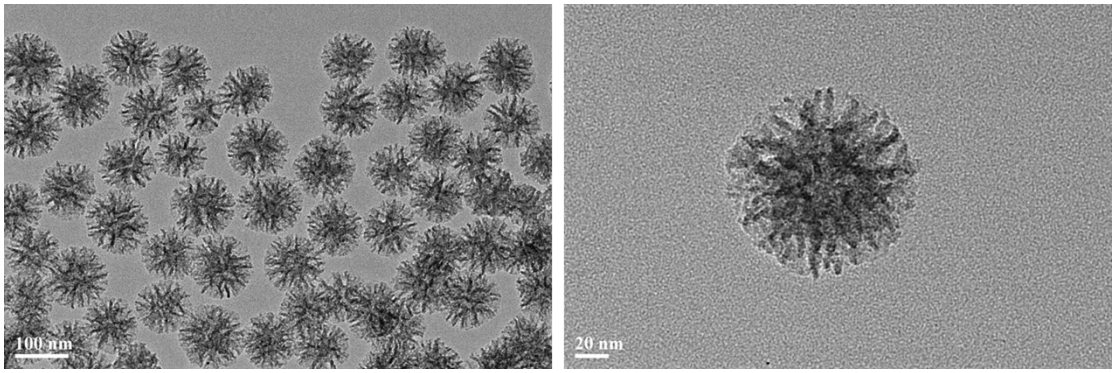

Figure S1. TEM images of DMSNs-Oct-SO_3H

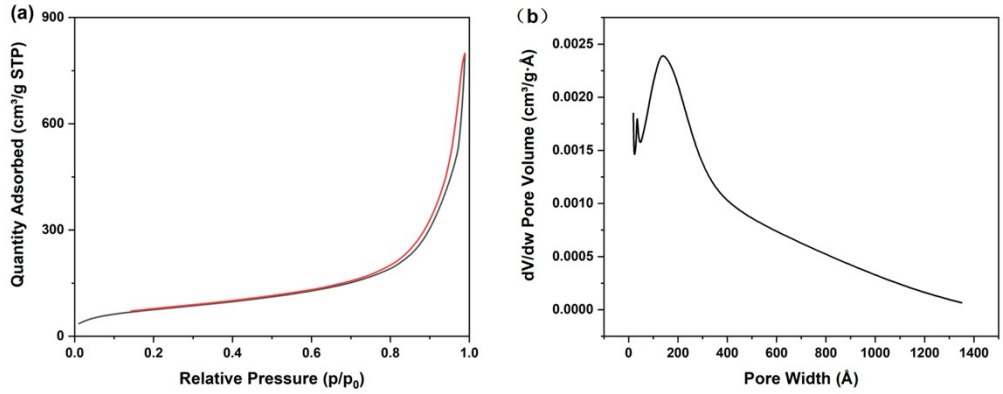

Figure S2. N_2 physisorption isotherms of the DMSNs-Oct-SO_3H (a) and their corresponding pore size distribution curve calculated by the BJH method (b).

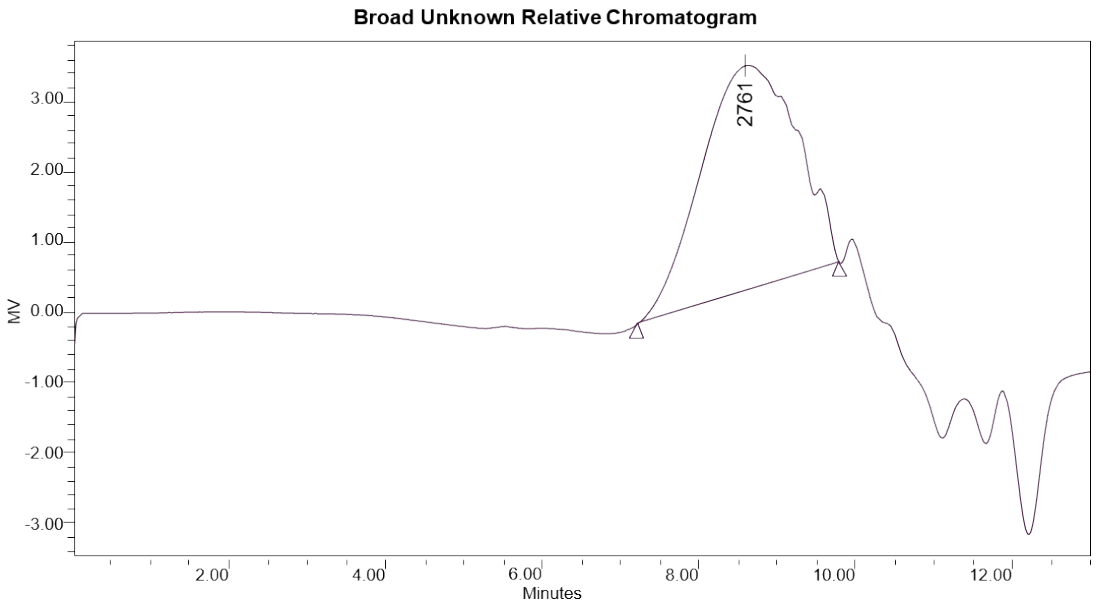

Broad Unknown Relative Peak Table

	Distribution Name	Mn (Daltons)	Mw (Daltons)	MP (Daltons)	Mz (Daltons)	Mz+1 (Daltons)	Polydispersity	Mz/Mw	Mz+1/Mw
1		2310	3109	2761	4095	5123	1.345586	1.317256	1.647726

Figure S3. GPC curve of PHDA from DMSNs-Oct-SO_3H-catalyzed polycondensation

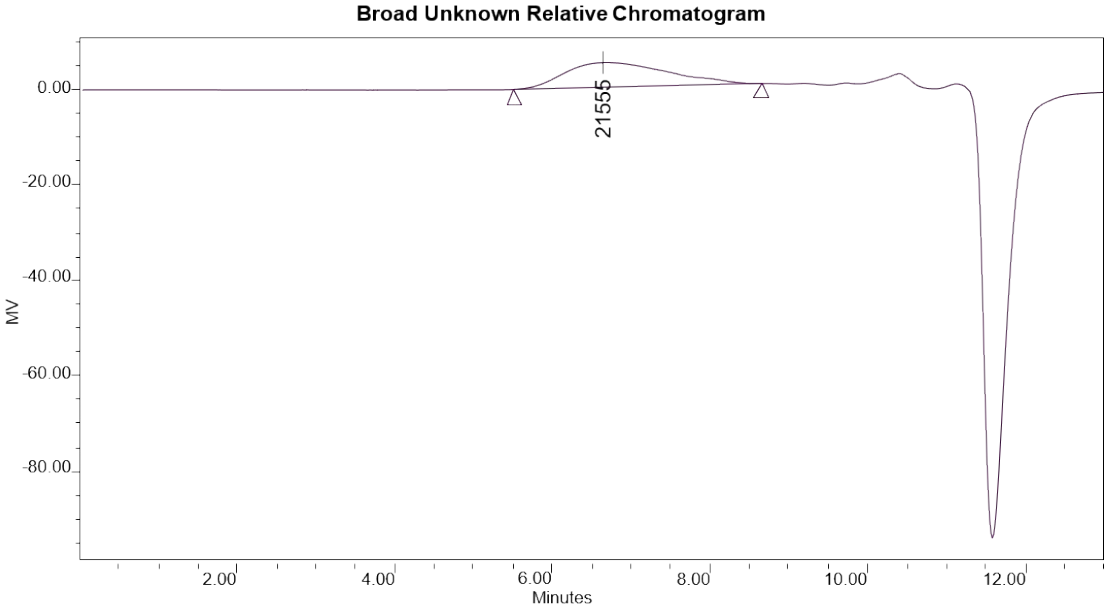

Broad Unknown Relative Peak Table

	Distribution Name	Mn (Daltons)	Mw (Daltons)	MP (Daltons)	Mz (Daltons)	Mz+1 (Daltons)	Polydispersity	Mz/Mw	Mz+1/Mw
1		13538	18831	21555	23846	27817	1.390947	1.266320	1.477176

Figure S4. GPC curve of PHDA from $TsOH \cdot H_2O$-catalyzed polycondensation

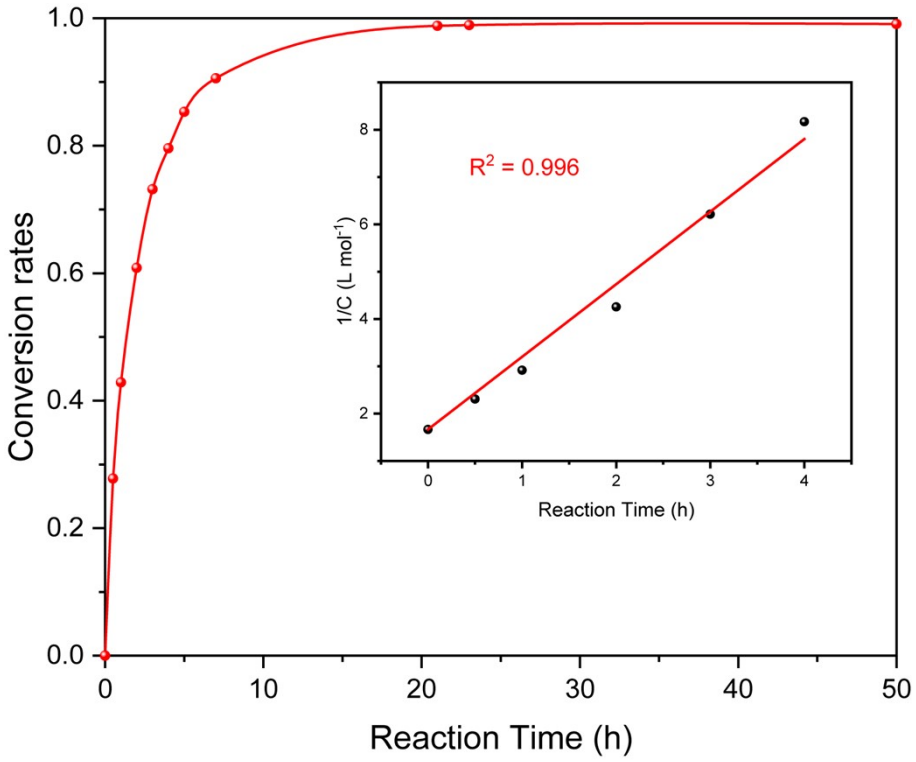

Figure S5. The conversion rates of 1,6-hexanediol was determined by GC at different time. The samples were dissolved in THF and Tetradecane as standard. Inset: the fitting plot of second-order reaction kinetics.

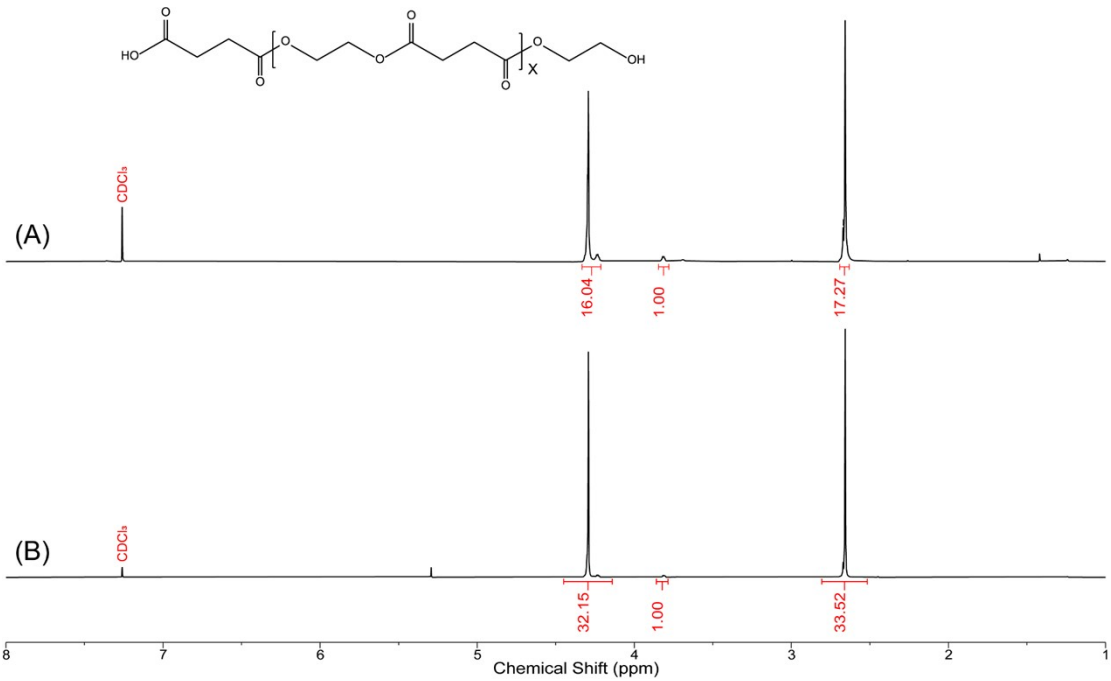

Figure S6. Comparison of ^{1}H NMR spectra of PE22 obtained from DMSNs-Oct-SO_3H (A) and $TsOH{\cdot}H_2O$ (B)-catalyzed polycondensation.

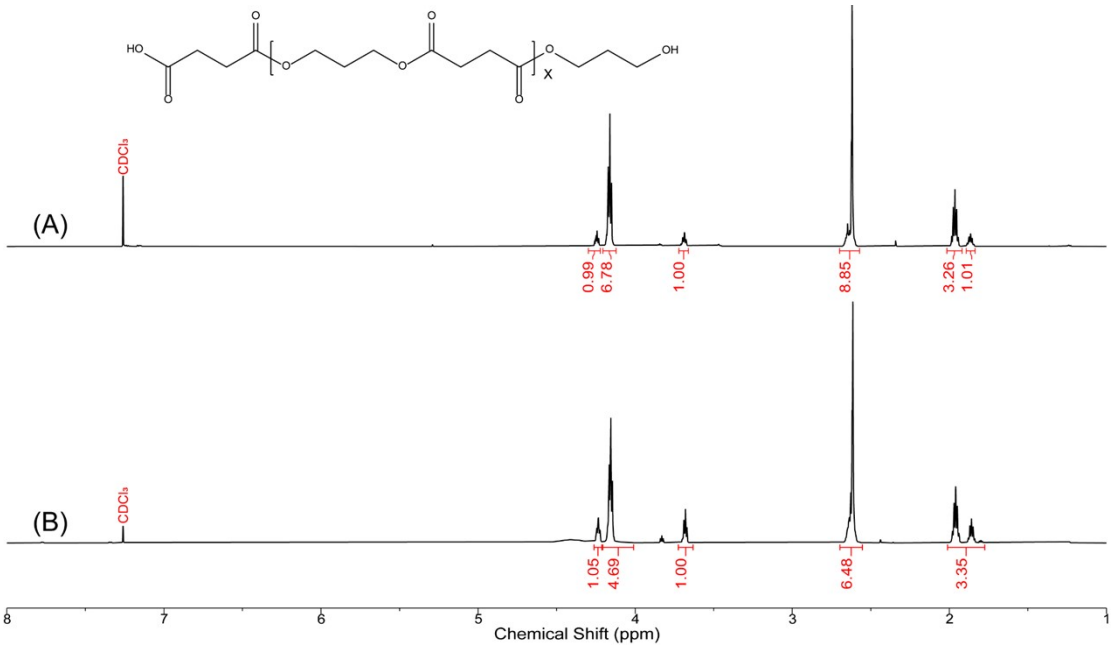

Figure S7. Comparison of ^{1}H NMR spectra of PE23 obtained from DMSNs-Oct-SO_3H (A) and $TsOH \cdot H_2O$ (B)-catalyzed polycondensation.

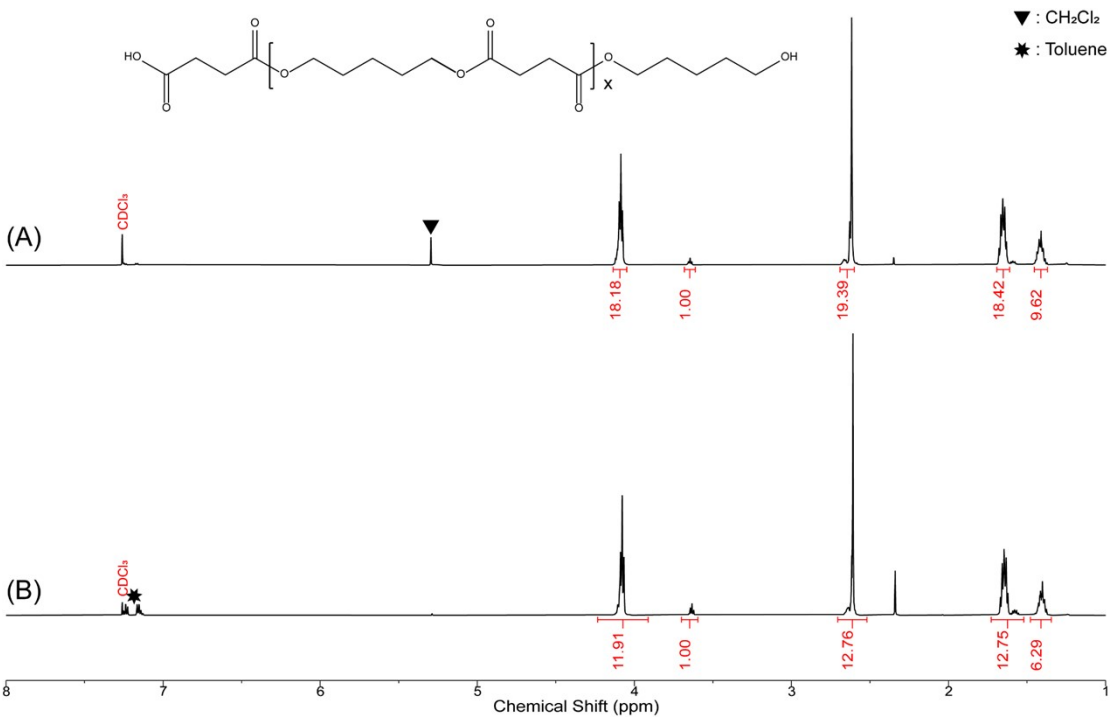

Figure S8. Comparison of ^{1}H NMR spectra of PE25 obtained from DMSNs-Oct-SO_3H (A) and $TsOH \cdot H_2O$ (B)-catalyzed polycondensation.

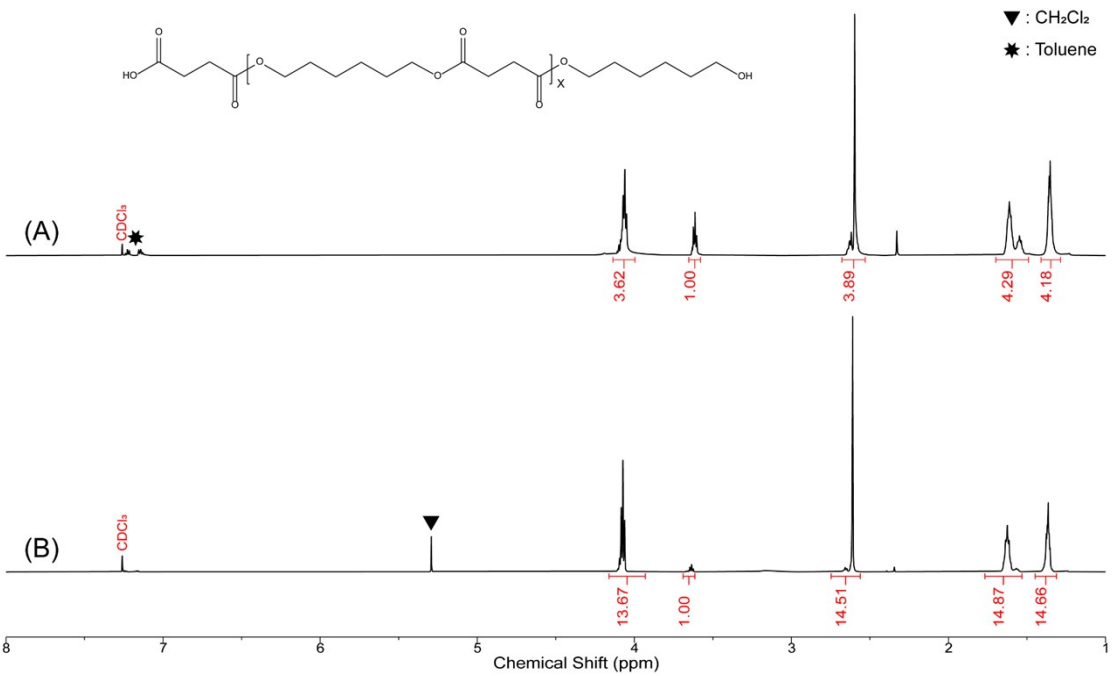

Figure S9. Comparison of ^{1}H NMR spectra of PE26 obtained from DMSNs-Oct-SO_3H (A) and $TsOH \cdot H_2O$ (B)-catalyzed polycondensation.

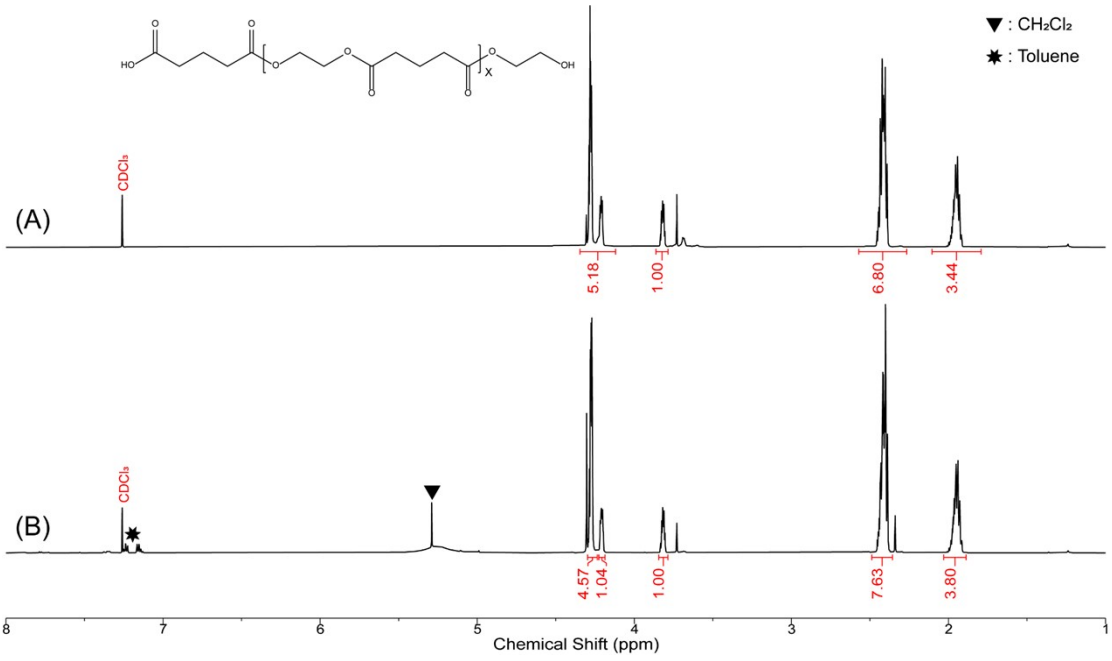

Figure S10. Comparison of ^{1}H NMR spectra of PE32 obtained from DMSNs-Oct-SO_3H (A) and $TsOH \cdot H_2O$ (B)-catalyzed polycondensation.

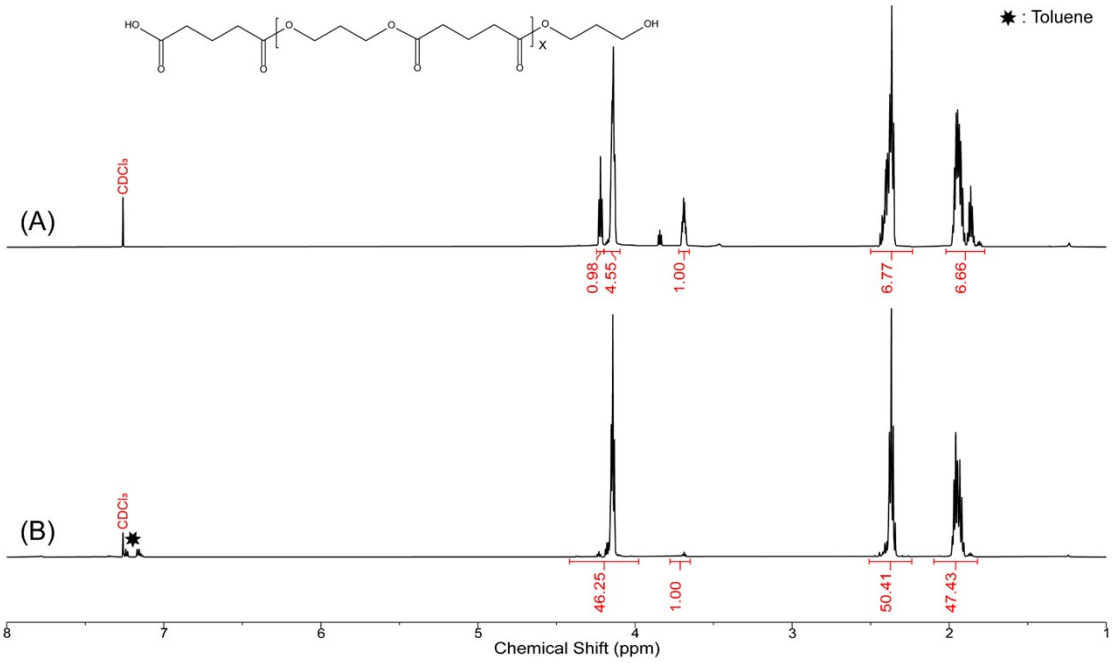

Figure S11. Comparison of ^{1}H NMR spectra of PE33 obtained from DMSNs-Oct-SO_3H (A) and $TsOH \cdot H_2O$ (B)-catalyzed polycondensation.

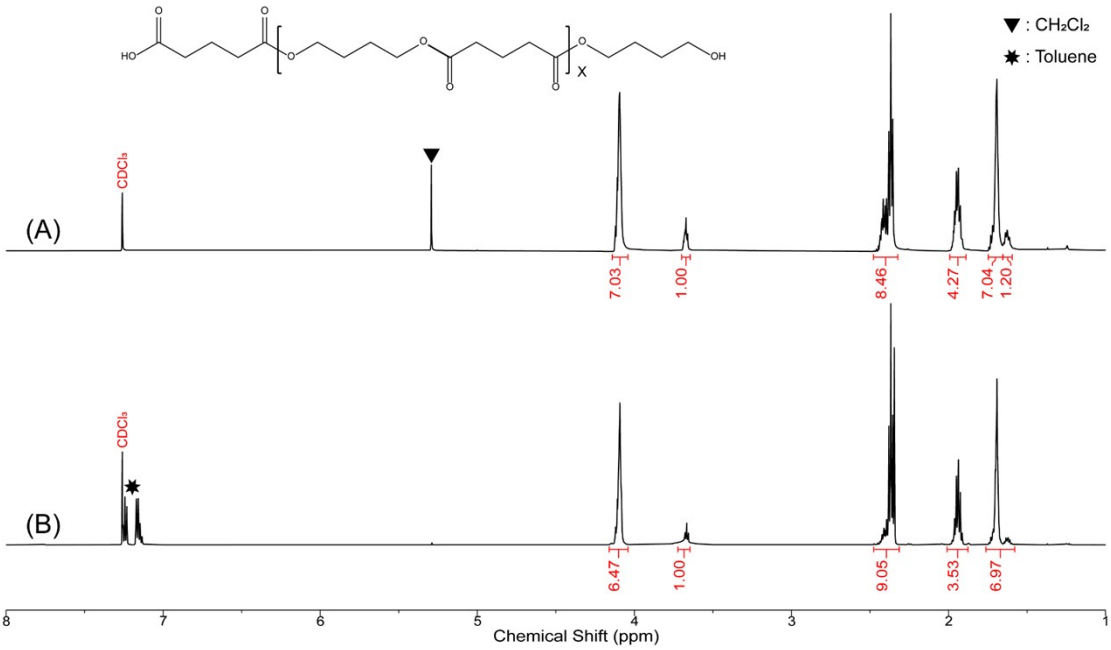

Figure S12. Comparison of ^{1}H NMR spectra of PE34 obtained from DMSNs-Oct-SO_3H (A) and $TsOH \cdot H_2O$ (B)-catalyzed polycondensation.

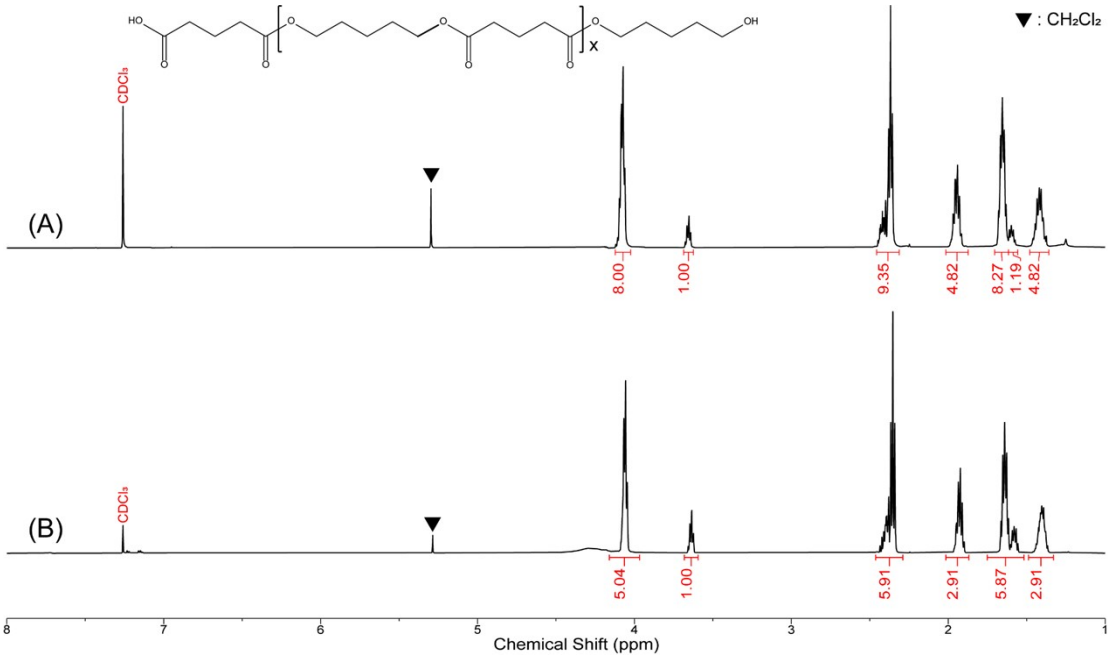

Figure S13. Comparison of ^{1}H NMR spectra of PE35 obtained from DMSNs-Oct-SO_3H (A) and $TsOH \cdot H_2O$ (B)-catalyzed polycondensation.

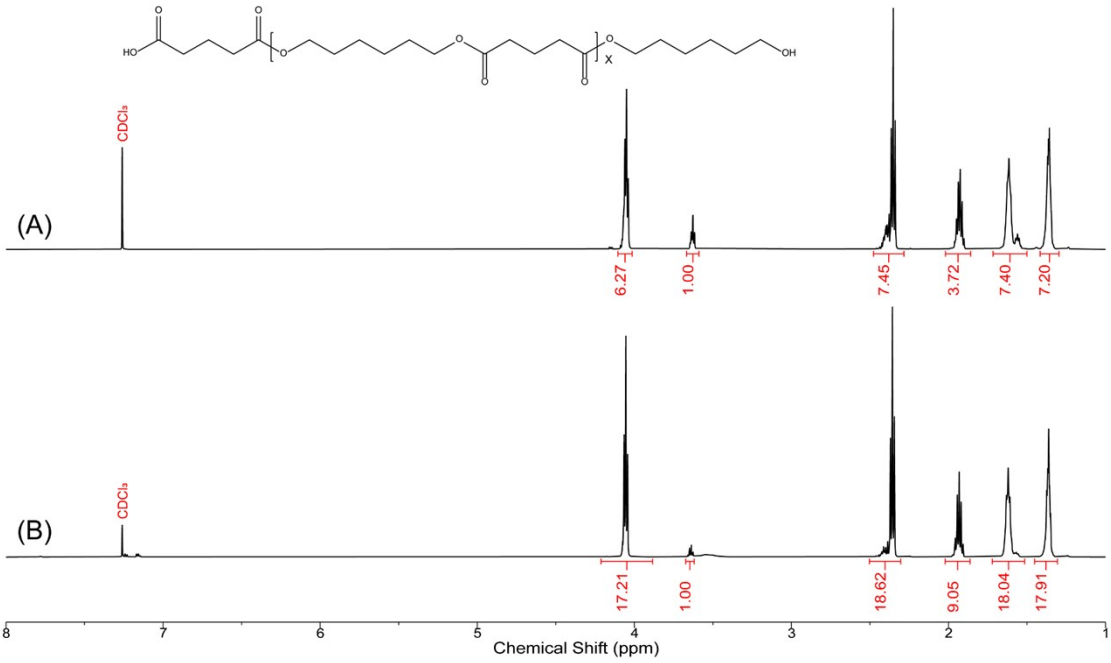

Figure S14. Comparison of ^{1}H NMR spectra of PE36 obtained from DMSNs-Oct-SO_3H (A) and $TsOH \cdot H_2O$ (B)-catalyzed polycondensation.

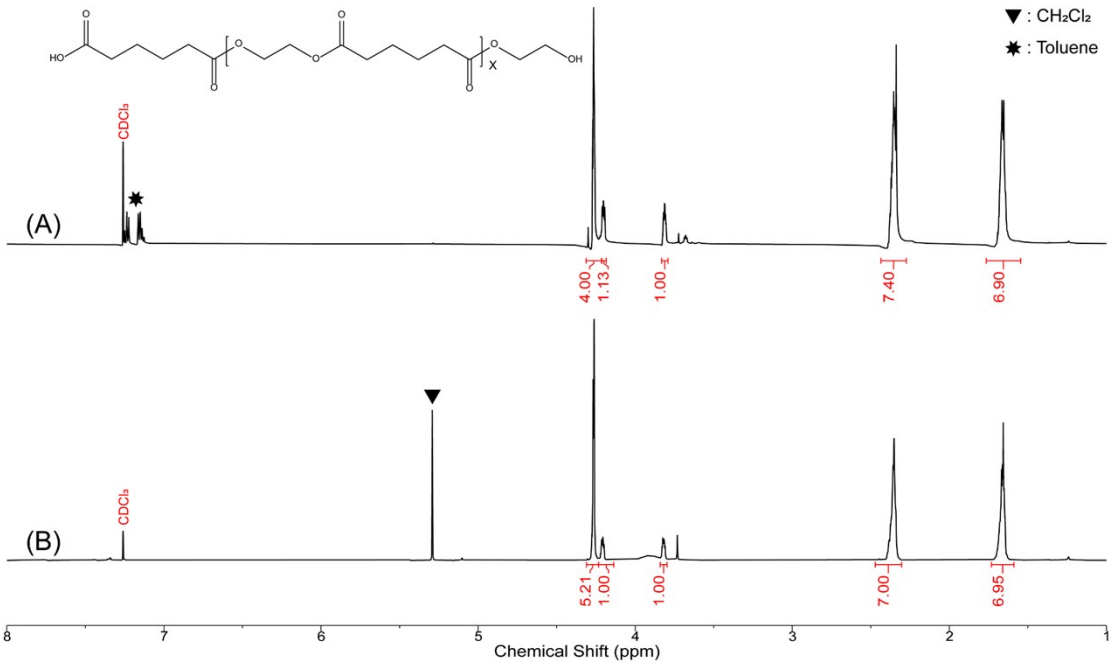

Figure S15. Comparison of ^{1}H NMR spectra of PE42 obtained from DMSNs-Oct-SO_3H (A) and $TsOH{\cdot}H_2O$ (B)-catalyzed polycondensation.

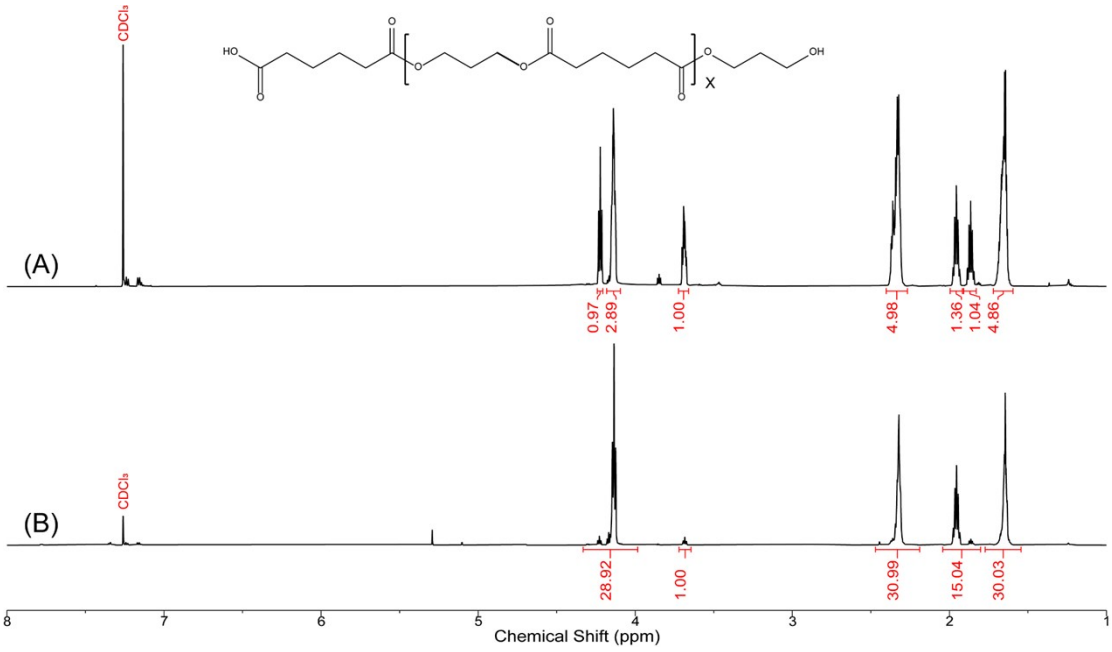

Figure S16. Comparison of ^{1}H NMR spectra of PE43 obtained from DMSNs-Oct-SO_3H (A) and $TsOH{\cdot}H_2O$ (B)-catalyzed polycondensation.

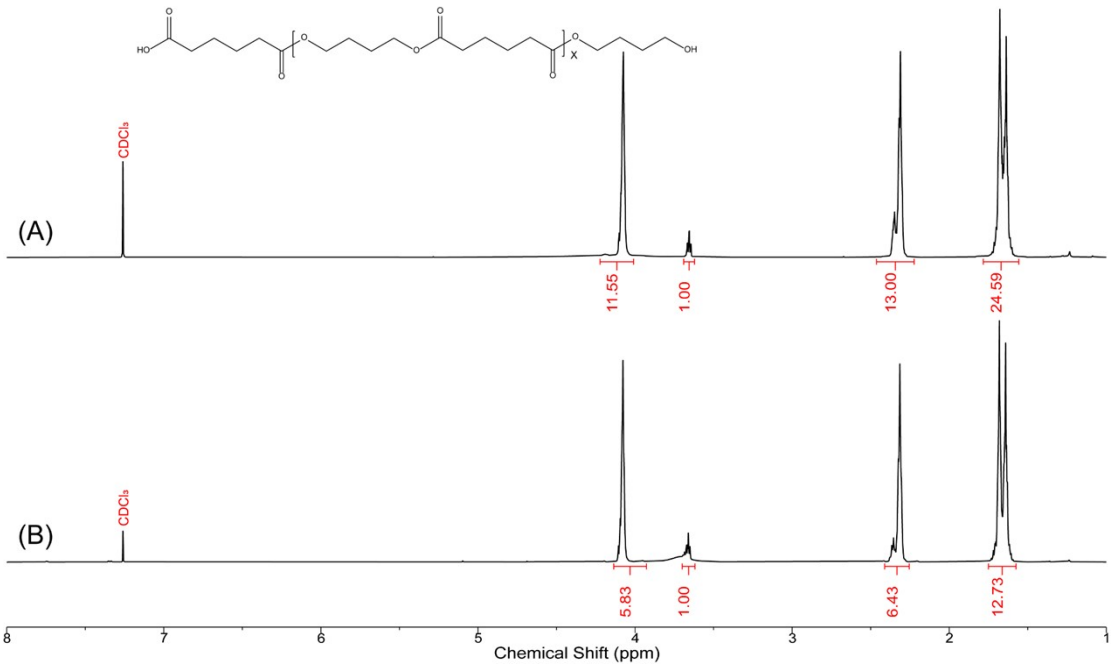

Figure S17. Comparison of ^{1}H NMR spectra of PE44 obtained from DMSNs-Oct-SO_3H (A) and $TsOH{\cdot}H_2O$ (B)-catalyzed polycondensation.

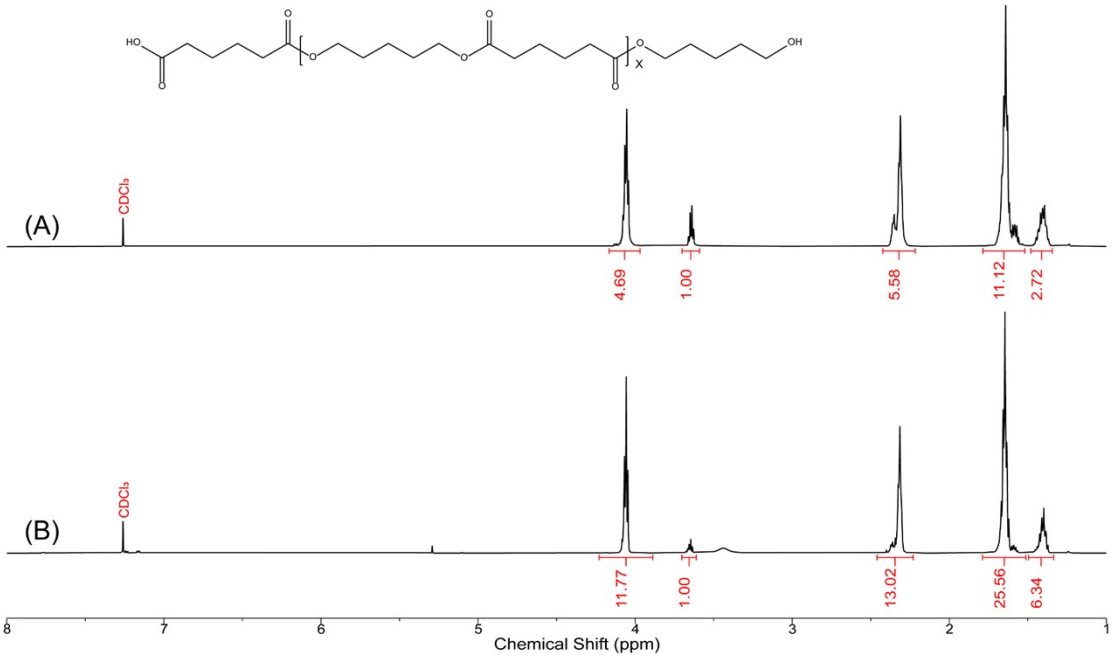

Figure S18. Comparison of ^{1}H NMR spectra of PE45 obtained from DMSNs-Oct-SO_3H (A) and $TsOH{\cdot}H_2O$ (B)-catalyzed polycondensation.

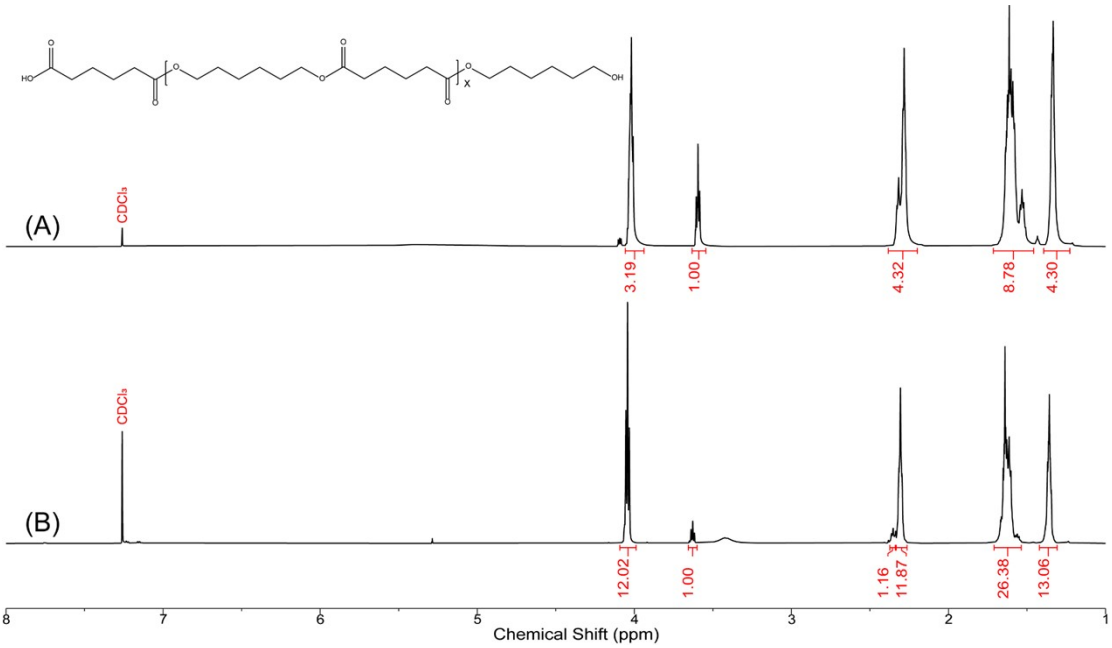

Figure S19. Comparison of ^{1}H NMR spectra of PE46 obtained from DMSNs-Oct-SO_3H (A) and $TsOH \cdot H_2O$ (B)-catalyzed polycondensation.

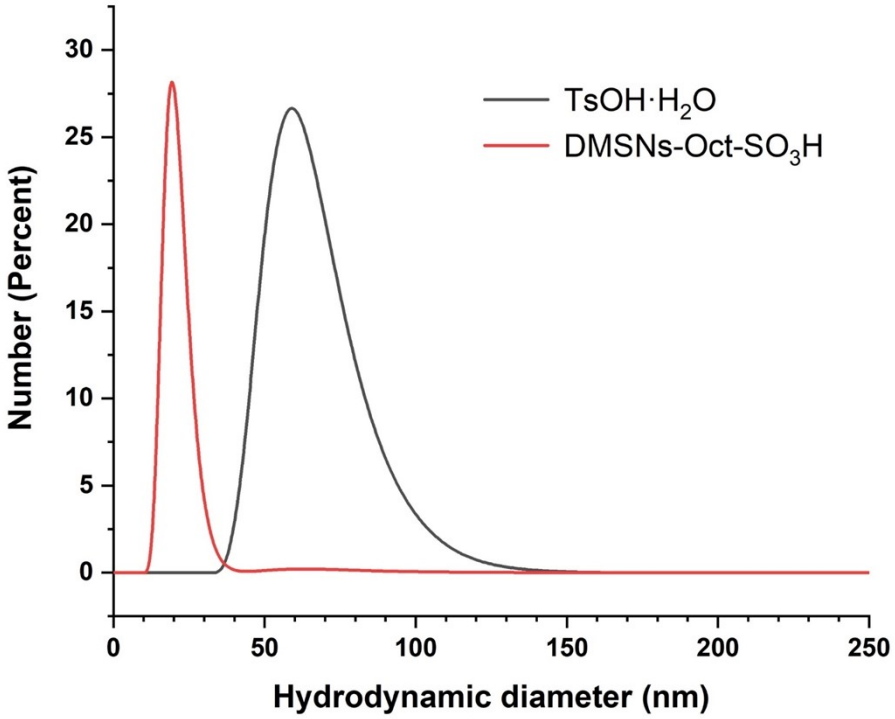

Figure S20. Hydrodynamic diameter of PHDAs obtained from DMSNs-Oct-SO_3H (red) and $TsOH \cdot H_2O$ (black)-catalyzed polycondensation measured by DLS analysis.